Chemical Engineering Journal 158 (2010) 458–467

Contents lists available at ScienceDirect

Chemical Engineering Journal

journal homepage: www.elsevier.com/locate/cej

Kinetic modeling of fluoride adsorption from aqueous solution onto bone char

R. Leyva-Ramos[a,*], J. Rivera-Utrilla[b], N.A. Medellin-Castillo[a], M. Sanchez-Polo[b]

[a] Centro de Investigacion y Estudios de Posgrado, Facultad de Ciencias Quimicas, Universidad Autonoma de San Luis Potosi, Av. Dr. M. Nava No. 6, San Luis Potosi SLP 78210, Mexico
[b] Departamento de Quimica Inorganica, Facultad de Ciencias, Universidad de Granada, 18071 Granada, Spain

ARTICLE INFO

Article history:
Received 19 July 2009
Received in revised form 11 January 2010
Accepted 12 January 2010

Keywords:
Adsorption
Bone char
Effective diffusivity
Fluoride
Tortuosity

ABSTRACT

The rate of fluoride adsorption from water solution on bone char was interpreted by using a diffusional model as well as kinetic models. The experimental data for the fluoride concentration decay were obtained in a rotating basket adsorber. The diffusional model considered that the overall rate of adsorption was due to the following steps: external mass transfer, intraparticle diffusion and adsorption on an active site. It was assumed that the rate of adsorption on the active sites was instantaneous. Furthermore, the overall rate of adsorption of fluoride was controlled by the pore volume diffusion. The diffusional model fitted the experimental concentration decay curves satisfactorily and the effective pore volume diffusivity of the fluoride in the bone char varied from 2.73×10^{-6} to 3.71×10^{-6} cm^2/s. The tortuosity factor of the bone char was estimated from the effective diffusivity of the fluoride and varied between 1.7 and 2.3. It was recommended to use an average tortuosity factor of $\tau_p = 2.1$ to estimate the effective diffusion coefficient of fluoride in bone char. The effective diffusivity of fluoride and the tortuosity factor were not dependent upon the operating conditions. The first-, second- and *n*th-order kinetic models were fitted to the experimental concentration decay data. The results revealed that the second- and the *n*th-order kinetic models adjusted the experimental data satisfactorily; nevertheless, the rate constants varied with the operating conditions without a reasonable trend. It was concluded that the diffusional model interpreted the experimental data better than the kinetic models.

1. Introduction

The level of fluoride in drinking water is a very important physicochemical factor which must be considered when assessing water quality for human consumption. The presence of fluoride in water for human consumption is important since it can be beneficial in preventing dental fluorosis at concentrations of 0.5 mg/L, but it can be detrimental to cause dental fluorosis at concentrations higher than 1.5 mg/L.

The concentration of fluoride in water for human consumption can be decreased below the permissible limit by the following methods: ion exchange on polymeric resins, adsorption, reverse osmosis and electrodialysis. The most commonly applied method is adsorption on activated alumina [1,2].

Bone char has been considered as a potential adsorbent for eliminating excessive fluoride in drinking water for human consumption [1–3]. Nevertheless, bone char has not been extensively applied because of problems related to the unpleasant taste and smell, and yellowish color of the treated water [1,2]. These problems were due to that the bone char still contained organic matter because the charring temperatures were below 500 °C. On the other hand, bone char produced at temperatures above 600 °C presented lower fluoride adsorption capacity than that charred at temperatures below 600 °C [4,5]. The adsorption capacity and quality of the bone char are highly dependent upon the charring temperature and time. Hence, the procedure for preparing bone char is decisive to optimize its application as a defluoridation adsorbent of drinking water. The bone char produced by partly calcination at a temperature of 550 °C and a charring time of 4 h, can be appropriate for defluoridation of drinking water [1].

Very few studies have been focused on the application of bone char for removing fluoride from water for human consumption. Abe et al. [6] and Medellin-Castillo et al. [7] investigated the adsorption of fluoride on bone char from water solutions. The adsorption capacity is considerably dependent upon the physicochemical properties of the bone char surface and the solution pH [7]. It has been found that the adsorption mechanism of fluoride on bone char is attributed to chemical and physical adsorption, the last is due to electrostatic interaction between the surface charge and the fluoride ions in solution [8].

At the industrial application, the adsorption of a given pollutant is mainly carried out in fixed bed adsorbers. To design these adsorbers, it is required to know the adsorption capacity and the overall rate of adsorption [9]. The first step in designing an adsorption pro-

* Corresponding author.
E-mail address: rlr@uaslp.mx (R. Leyva-Ramos).

1385-8947/$ – see front matter © 2010 Elsevier B.V. All rights reserved.
doi:10.1016/j.cej.2010.01.019

Nomenclature

a	Prausnitz–Radke isotherm constant (L/g)
b	Prausnitz–Radke isotherm constant $(L/mg)^{\beta}$
C	concentration of fluoride at equilibrium (mg/L)
C_A	concentration of fluoride in aqueous solution (mg/L)
C_{A_0}	initial concentration of fluoride in aqueous solution (mg/L)
C_{A_e}	final concentration of fluoride at equilibrium in solution (mg/L)
$C_{A,r}$	concentration of fluoride in the pore volume at a distance r (mg/L)
$C_{A,R}$	concentration of fluoride in aqueous solution at the external surface of bone char ($r = R$) (mg/L)
$D_{e,p}$	effective pore volume diffusivity (cm^2/s)
$D^{\circ}_{Na^+}$	molecular diffusion coefficient of sodium ion at a dilute concentration (cm^2/s)
$D^{\circ}_{F^-}$	molecular diffusion coefficient of fluoride ion at a dilute concentration (cm^2/s)
D_{F^-}	ionic diffusivity of fluoride in aqueous solution (cm^2/s)
k	Freundlich isotherm constant $(L^{1/nf}/(mg^{1/nf-1}\,g))$
K	Langmuir isotherm constant (L/mg)
k_1	rate constant for the first-order reaction (min^{-1})
k_2	rate constant for the second-order reaction ($g\,mg^{-1}\,min^{-1}$)
k_L	external mass transfer coefficient in liquid solutions (cm/s)
k_n	rate constant for the nth-order reaction ($g^{n-1}\,mg^{1-n}\,min^{-1}$)
m	mass of bone char (g)
n	nth-order reaction
nf	Freundlich isotherm constant
N	number of experimental data points
q	mass of fluoride adsorbed per unit mass of bone char (mg/g)
q_{pred}	mass of fluoride adsorbed predicted with the isotherm model (mg/g)
q_e	mass of fluoride adsorbed at equilibrium (mg/g)
q_{exp}	experimental mass of fluoride adsorbed (mg/g)
q_m	Langmuir isotherm constant (mg/g)
r	distance in radial direction of a bone char particle (cm)
R	radius of a bone char particle (cm)
S	external surface of the particles of bone char per unit mass of bone char (cm^2/g)
t	time (min)
V	volume of the fluoride solution (mL)
β	Prausnitz–Radke isotherm constant
ε_p	void fraction of bone char
ϕ	dimensionless concentration of fluoride in solution
ϕ_{exp}	experimental dimensionless concentration of fluoride in solution
ϕ_{pred}	dimensionless concentration of fluoride in solution predicted with the models
ρ_p	density of bone char particles (g/mL)
τ_p	Tortuosity factor of bone char

cess is to find an adsorbent with a high capacity, high selectivity, and long life. Furthermore, this adsorbent must be available in large amounts as well as inexpensive. The second step is to choose an adsorbent in which the overall rate of adsorption is fast [10].

In analyzing the overall rate of adsorption, it is fundamental to study the mass transport mechanisms and parameters representing these mechanisms. Normally, these parameters are the external mass transfer coefficient in the liquid phase and the effective intraparticle diffusion coefficient. The overall adsorption rate of a solute or adsorbate from a solution to the active sites of a porous adsorbent may be interpreted with a diffusional model that consists of three steps [11]: (1) external mass transport, (2) intraparticle diffusion and (3) adsorption rate on an active site.

Very few studies have been reported on the rate of adsorption from water solution onto bone char. The adsorption rates of Cu^{2+}, Cd^{2+} and Zn^{2+} on bone char have been investigated using kinetic models [12,13] as well as diffusional models [14–17]. A literature review revealed the rate of fluoride adsorption on bone char has not been studied.

The adsorption rate of fluoride on various adsorbents has been investigated by several authors. The adsorption rate of fluoride on coke, lignite, and bituminous carbon was interpreted using the kinetic models of pseudo-first-order and pseudo-second-order, and it was found that the kinetics of fluoride adsorption can be satisfactorily predicted with a pseudo-first-order kinetic model [18], and the first-order kinetic constant was directly proportional to the surface area of these adsorbents. The kinetics of fluoride adsorption on activated alumina and alumina cement [19–21] has been modeled using kinetic models as well as an intraparticle diffusion model. Ku and Chiou [19] assumed that the adsorption rate was controlled by a surface reaction and proposed a second-order kinetic model, which was first-order regarding the concentration of fluoride in the aqueous solution and first-order with the concentration of unoccupied active sites on the activated alumina surface. This kinetic model matched satisfactorily the experimental data. Ayoob et al. [20] reported that the adsorption rate of fluoride on alumina cement particles was suitably described by a kinetic model of pseudo-second-order. On the other hand, Ghorai and Pant [21] found that the adsorption rate of fluoride on activated alumina was fast in the first 6 h and decreased slowly afterwards. The experimental rate of adsorption data was interpreted with a first-order kinetic model. However, an intraparticle diffusional model also fitted the experimental data. The authors concluded that surface reaction rate and intraparticle diffusion contributed to the overall adsorption rate of fluoride on activated alumina.

The aim of this work was to study the adsorption rate of fluoride on bone char using kinetic models as well as a diffusional model. The diffusional model incorporated the external mass transfer and intraparticle diffusion. The concentration decay curves predicted with the diffusional model were compared with those with the kinetic models. The effects of the operating conditions on the rate of adsorption were also investigated. The advantages of each model were argued and a model was selected to predict the overall rate of adsorption of fluoride on bone char.

2. Diffusional model

In the diffusional model, the overall adsorption rate of fluoride on bone char is assumed to take place by a mechanism consisting of three consecutive steps: (i) external mass transport, (ii) intraparticle diffusion, and (iii) adsorption rate on a site inside the pores [9].

The diffusional model interprets the adsorption rate in a batch adsorber that contains a certain mass of bone char, and a constant volume of an aqueous solution with a known initial fluoride concentration. The adsorption system is composed of two phases: the constant volume solution of fluoride and the porous particles of bone char. The diffusional model was developed by performing mass balances of fluoride in each phase. The following assumptions

were made: (i) intraparticle diffusion is exclusively due to diffusion in the pore volume (Fick diffusion), and (ii) the rate of adsorption on an active site is instantaneous.

The ordinary and partial differential equations representing the diffusional model are [9]:

$$V\frac{dC_A}{dt} = -mSk_L(C_A - C_{A,R}) \quad (1)$$

$$\varepsilon_p\frac{\partial C_{A,r}}{\partial t} + \rho_p\frac{\partial q}{\partial t} = \frac{1}{r^2}\frac{\partial}{\partial r}\left[r^2\left(D_{e,p}\frac{\partial C_{A,r}}{\partial r}\right)\right] \quad (2)$$

The initial and boundary conditions necessary for solving these differential equations are:

$$t = 0, \qquad C_A = C_{A_0} \quad (3)$$

$$t = 0, \qquad C_{A,r} = 0, \quad 0 \le r \le R \quad (4)$$

$$\left.\frac{\partial C_{A,r}}{\partial r}\right|_{r=0} = 0 \quad (5)$$

$$D_{e,p}\left.\frac{\partial C_{A,r}}{\partial r}\right|_{r=R} = k_L(C_A - C_{A,R}) \quad (6)$$

If the adsorption rate of fluoride on an active site is assumed to be instantaneous then, local equilibrium exists between the fluoride in the solution inside the pore and the fluoride adsorbed on an active site. This equilibrium can be represented by the adsorption isotherm, which is a mathematical relation between $C_{A,r}$ and q. The adsorption isotherm can be expressed as:

$$q = f(C_{A,r}) \quad (7)$$

The partial and ordinary differential equations of this model were numerically solved by using the PDESOL software.

3. Kinetic models

In the literature several kinetic models have been reported for interpreting the overall adsorption rate of a pollutant on a porous solid adsorbent [22]. In contrast to the diffusional models, the overall rate of adsorption in the kinetic models is not considered to be controlled by any of the mass transport mechanisms, but rather by the surface adsorption rate. The overall rate of adsorption is represented in a similar fashion as the rate of a chemical reaction.

The kinetic adsorption models are obtained by performing an overall mass balance of the adsorbate:

$$m\frac{dq}{dt} + V\frac{dC_A}{dt} = 0 \quad (8)$$

In this equation, it is considered that there are no concentration gradients existing within the particles of the adsorbent. Therefore, the intraparticle diffusion and the external mass transport are neglected since they are much faster than the adsorption rate on the surface. Eq. (8) is integrated by using the initial condition $q = 0$ at $t = 0$ and the next equation is obtained:

$$q = \frac{V(C_{A_0} - C_A)}{m} \quad (9)$$

The first-order adsorption rate is expressed as [22]:

$$\frac{dq}{dt} = k_1(q_e - q) \quad (10)$$

This equation is integrated by using the above initial condition and the resulting equation is:

$$q = q_e(1 - e^{-k_1 t}) \quad (11)$$

This equation can be expressed in terms of C_A and C_{A_e} using Eq. (9) and the resulting equation is:

$$C_A = C_{A_e} + (C_{A_0} - C_{A_e})e^{-k_1 t} \quad (12)$$

The adsorption rate for a second-order adsorption reaction can be represented by the following equation [22]:

$$\frac{dq}{dt} = k_2(q_e - q)^2 \quad (13)$$

By integrating this equation, the following one is obtained:

$$\frac{1}{(q_e - q)} - \frac{1}{q_e} = k_2 t \quad (14)$$

Expressing the above equation in terms of C_A and C_{A_e}, the final equation is:

$$C_A = C_{A_0} - \left(\frac{m}{V}\right)\frac{k_2[(V/m)(C_{A_0} - C_{A_e})]^2 t}{(1 + k_2[(V/m)(C_{A_0} - C_{A_e})]t)} \quad (15)$$

The adsorption rate for an n-order is represented as follows:

$$\frac{dq}{dt} = k_n(q_e - q)^n \quad (16)$$

Now, this equation can be related to C_A and C_{A_e}, and the result is:

$$\frac{dC_A}{dt} = -k'_n(C_A - C_{A_e})^n \quad (17)$$

The relationship between k_n and k'_n is given by the following equation:

$$k'_n = \left(\frac{V}{m}\right)^{n-1} k_n \quad (18)$$

4. Materials and methods

4.1. Bone char

The bone char used in this study is commercially known as Fija Fluor and manufactured from animal bones by the APELSA, Guadalajara, Mexico. The bone char was sieved to the average particle diameters of 0.65, 0.79 and 1.29 mm, washed several times with deionized water, dried in a furnace at 100 °C for 24 h and stored in plastic containers.

4.2. Properties of bone char

The textural and physicochemical properties of the bone char were reported in a previous work [7]. The surface area, pore volume and average pore diameter were 104 m^2/g, 0.30 cm^3/g and 11.1 nm, respectively. The concentrations of acid and basic sites were 0.29 and 0.62 mequiv./g, respectively.

4.3. Determination of the fluoride concentration in aqueous solution

The concentration of fluoride in an aqueous solution was determined by a potentiometric method. The potential was measured using an SA 720, Orion model, potentiometer with a fluoride ion selective electrode. The concentration of the fluoride in a sample was determined with a calibration curve, concentration of fluoride vs. potential. The calibration curve was prepared with eight standard solutions with concentrations ranging from 0.1 to 10 mg/L. The experimental error in determining the fluoride concentration was estimated to be less than 0.5%.

4.4. Adsorption equilibrium data

The experimental adsorption equilibrium data were obtained in a 500-mL Erlenmeyer flask that served as the batch adsorber. The procedure is described as follows. A fluoride solution of an initial concentration varying from 1 to 20 mg/L, was prepared in a 500-mL volumetric flask, the pH of this solution was adjusted to pH 7 and a 20-mL sample was taken, which was later analyzed to corroborate the initial concentration. The solution was transferred to the batch adsorber, which was then partially submerged in a thermostatic water bath. A Nylon basket containing 0.5 or 1 g of the bone char was placed inside the solution in the batch adsorber. The solution was stirred continuously at 200 rpm with a Teflon-coated stirring bar and a magnetic stirrer placed under the thermostatic bath. The bone char and solution were left in contact until equilibrium was reached. The solution pH was periodically measured using a potentiometer and kept constant at pH 7 by adding 0.01, 0.1 and 1.0 M HNO_3 or NaOH solutions as required. The volumes of these solutions were registered to estimate the final total volume of the solution. The solution was sampled at certain times and the concentration of fluoride in each sample was determined by the electroanalytical method described earlier. It was considered that equilibrium had been attained when the concentrations of two successive samples did not vary significantly. In preliminary runs, it was found that 7 days were enough to reach equilibrium. The mass of fluoride adsorbed was estimated by performing a mass balance of fluoride. The experimental error in the mass of fluoride adsorbed was assessed to be less than 2%.

4.5. Rotating basket batch adsorber

The experimental adsorption rate data were obtained in a rotating basket batch adsorber that was similar to a Carberry reactor [23]. The adsorber consisted of a three-neck reaction flask and was equipped with four equally spaced baffles. The solution in the adsorber was mixed with an impeller, which was fixed through the central neck of the reaction flask and was turned on by a variable-speed motor. The blades of the impeller were replaced by two cylindrical baskets made from stainless steel mesh. The baskets had a capacity for 4 g of adsorbent and were 1.5 cm in diameter and 4 cm in length. One of the two-side necks of the flask was used for sampling or adding a make-up solution, and the other neck was employed for introducing a thermometer. The temperature of the adsorber solution was kept constant by partially submerging the adsorber in a constant temperature water bath.

4.6. Method for obtaining the rate of adsorption data

The experimental concentration decay curves for the fluoride adsorption on bone char were obtained in a rotating basket adsorber. First, a solution was prepared by mixing equal volumes of 0.01 M HNO_3 and NaOH solutions and the solution pH was adjusted to 7. This solution was transferred to a 1-L volumetric flask. Next, an aliquot of a certain volume was taken and the remaining solution was added to the adsorber. Moreover, the baskets were packed with a certain mass of bone char and were attached to the impeller, and the impeller was then set up in the adsorber. The motor of the impeller was turned on and the bone char and the solution were left in contact for 2 days. The pH of the solution was periodically measured and adjusted to 7 by adding 0.1 M HNO_3 solution. Once the pH of the solution in the adsorber did not vary over time, an aliquot of a solution of known concentration of fluoride was added to the adsorber and the volume of this aliquot must be equal to that taken from the 1-L volumetric flask. Immediately afterwards, the timer was turned on and the time was registered as $t = 0$. During the whole experiment, the pH of the solution was periodically measured by a potentiometer and adjusted by adding 0.1 M HNO_3 solution. The fluoride concentration decay curve was obtained by sampling the solution in the adsorber at different times. Immediately after taking a sample, an equal volume of a make-up solution of fluoride was added. The concentration of fluoride in the make-up solution was close to the average of the initial and final equilibrium concentrations of fluoride in the adsorber solution. The reason for the addition was to restitute the mass of fluoride that was taken out with each sample. In this way, the volume of the solution in the adsorber was kept constant.

The experimental concentration decay data, concentration of fluoride vs. time, were expressed in dimensionless form by defining the following variable:

$$\phi = \frac{C_A}{C_{A_0}} \tag{19}$$

The dimensionless concentration, ϕ, was plotted against the time to obtain the dimensionless concentration decay curve.

5. Results and discussion

5.1. Adsorption isotherm

The experimental adsorption equilibrium data of fluoride on bone char at $T = 25\,^{\circ}C$, pH 7 and different particle diameters were interpreted using the Freundlich, Langmuir and Prausnitz–Radke isotherms. These isotherms are mathematically represented by the following equations:

$$q = k\,C^{1/\mathrm{nf}} \tag{20}$$

$$q = \frac{q_m KC}{1 + KC} \tag{21}$$

$$q = \frac{aC}{1 + bC^{\beta}} \tag{22}$$

The constants of these isotherms were estimated by employing a least-squares method based on the Rosenbrock–Newton optimization algorithm and the values of these constants at $T = 25\,^{\circ}C$ and pH 7 are listed in Table 1. Also, the average absolute percentage deviation, %D, was calculated by applying the following equation:

$$\%D = \frac{1}{N}\sum_{i=1}^{N}\left|\frac{q_{\mathrm{exp}} - q_{\mathrm{pred}}}{q_{\mathrm{exp}}}\right| \times 100\% \tag{23}$$

The values of %D are also included in Table 1. The data was best fitted with the Prausnitz–Radke isotherm because in all the cases the %D of this isotherm was always lower than those of the other two isotherms. The adsorption of fluoride on bone char was studied

Table 1
Freundlich, Langmuir and Prausnitz–Radke isotherms constants for the fluoride adsorption on bone char at pH 7 and $T = 25\,^{\circ}C$.

d_p (mm)	Freundlich			Langmuir			Prausnitz–Radke			
	k ($L^{1/nf}/(mg^{1/nf-1}\,g)$)	nf	%D	$q_m K$ (L/g)	K (L/mg)	%D	a (L/g)	b $(L/mg)^{\beta}$	β	%D
0.65	2.84	3.05	16.0	6.61	1.16	3.49	8.52	4.78	0.92	1.30
0.79	2.72	3.46	2.71	6.66	1.22	9.61	42.0	3.07	0.76	2.15
1.29	1.95	2.30	13.9	2.65	0.45	4.50	3.05	4.85	0.92	4.32

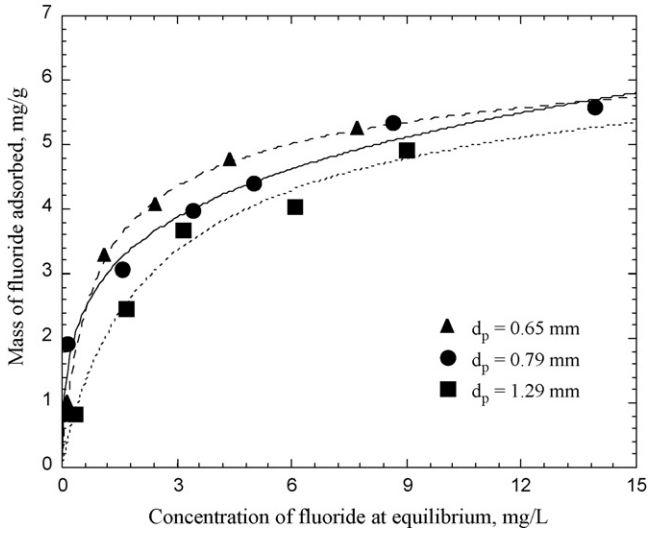

Fig. 1. Adsorption isotherms of fluoride on bone char at pH 7 and $T = 25\,^{\circ}C$. The lines represent the Prausnitz–Radke isotherms.

thoroughly in a previous work [7]. The effects of the solution pH and temperature as well as the bone char surface properties on the adsorption of fluoride on bone char have already been presented in a previous work [7].

The experimental data and the Prausnitz–Radke isotherm model for different particle diameters are graphed in Fig. 1. It can be seen in this figure that the adsorption capacity of the bone char increases slightly when the particle diameter is reduced by grinding. This effect cannot be due to the rate of adsorption since enough time was allowed to reach equilibrium. However, it may be attributed to that the fluoride ions could not enter all the pores and some of these unexposed pores were probably opened up while grinding the particle. In other words, the adsorption capacity was increased because some additional surface area was available for fluoride adsorption when the particles were ground. A similar effect had been reported for the adsorption of phenol on granular activated carbon [24].

5.2. Concentration decay curves of fluoride

In a previous work [7], it was found that the fluoride adsorption capacity of bone char was highly dependent on the solution pH and increased by diminishing the solution pH. For this reason, the solution pH had to be kept constant during the adsorption rate experiments; otherwise the adsorption capacity of bone char would have changed as adsorption progressed.

At the beginning of the adsorption rate experiment, it was observed that if the initial pH were below 7, the solution pH increased immediately, and it was difficult to keep constant the solution pH by adding 0.01 M HNO_3 solution. On the other hand, the solution pH varied slightly during adsorption at an initial pH of 7, and it was feasible to keep constant the solution pH. Thus, all experimental data for the fluoride concentration decay curves were obtained at pH 7.

The total volume of the solution added for maintaining constant the pH was always less than 2 cm^3; this volume represents only 0.2% of the total volume of the solution in the rotating basket adsorber. Thus, the total volume of the solution was considered to remain constant throughout the rate of adsorption experiments.

5.3. Molecular diffusion coefficient of fluoride

All the fluoride solutions were prepared by dissolving NaF, which dissociated into Na^+ and F^- ions. In this case, it was considered that the sodium fluoride solutions were quite dilute since the fluoride concentrations were less than 20 mg/L (1.05 mM). The diffusion coefficients of these ions in dilute aqueous solutions are reported in the literature at 25 °C and the values are as follows [25]: $D^0_{Na^+} = 1.334 \times 10^{-5}\,cm^2/s$ and $D^0_{F^-} = 1.475 \times 10^{-5}\,cm^2/s$. The ionic diffusivity of fluoride, D_{F^-}, was estimated from the following equation [26]:

$$D_{F^-} = \frac{(z_+ + |z_-|)D^0_{Na^+}D^0_{F^-}}{z_+ D^0_{Na^+} + |z_-|D^0_{F^-}} \tag{24}$$

where z_+ and z_- are the values of the positive and negative charges of the ions involved. Substituting values in the preceding equation, the ionic diffusivity of fluoride in aqueous solution is $D_{F^-} = 1.39 \times 10^{-5}\,cm^2/s$.

5.4. Mass transfer coefficient

The external mass transfer coefficient, k_L, was estimated using the method proposed by Furusawa and Smith [27]. This method is based on the mass balance equation of fluoride in the adsorber solution, Eq. (1). Evaluating this equation at the initial condition: $t = 0$, $C_A = C_{A_0}$ and $C_{A,R} = 0$, the following equation is obtained:

$$k_L = -\left(\frac{V}{mSC_{A_0}}\right)\left.\frac{dC_A}{dt}\right|_{t=0} = -\frac{\alpha R}{3C_{A_0}}\left(\frac{dC_A}{dt}\right)_{t=0} \tag{25}$$

The last term is the slope of the concentration decay curve at the beginning of the experiment ($t = 0$). This slope was estimated by using the first two concentration data points at $t = 0$ and $t = 15$ min and the following equation:

$$\left.\frac{dC_A}{dt}\right|_{t=0} = \frac{C_A - C_{A_0}}{t - 0} \tag{26}$$

The values of k_L are displayed in Table 2 and range between 0.37×10^{-3} and 3.07×10^{-3} cm/s. These values are within the range of experimental values of k_L obtained in a rotating basket adsorber for the adsorption of heavy metals on activated carbon [9] and organic compounds on activated carbon [28].

5.5. Interpretation of adsorption rate data with the diffusional model

The experimental data of the concentration decay curves of fluoride were interpreted with the diffusional model. The only two mass transfer parameters of this model are the external mass transfer coefficient, k_L, and the effective pore volume diffusivity, $D_{e,p}$. The external mass transfer coefficient was estimated as described in the previous section.

The $D_{e,p}$ was estimated by matching the experimental dimensionless concentration decay data, ϕ_{exp}, with the dimensionless concentration decay predicted with a numerical solution of the diffusional model, ϕ_{pred}. In the diffusional model, it was further assumed that the diffusion in the pore volume is the only intraparticle diffusion mechanism. The best value of $D_{e,p}$ was obtained when the diffusional model best fitted the experimental data, considering that the optimum fitting was achieved by minimizing the following objective function:

$$\text{Minimum} = \sum_{i=1}^{N}(\phi_{exp} - \phi_{pred})^2 \tag{27}$$

Figs. 2 and 3 show the experimental data of the fluoride concentration decay curves on bone char as well as the concentration decay predicted with the diffusional model. In all the cases, the diffusional model satisfactorily represented the experimental data.

Table 2
Experimental conditions of the concentration decay curves for the adsorption of fluoride on bone char at $T = 25\,^{\circ}C$ and pH 7. Mass transfer parameters of the diffusional model.

Run No.	d_p (mm)	Speed (rpm)	C_{A_0} (mg/L)	m (g)	C_{A_e} (mg/L)	q_e (mg/g)	k_L ($\times 10^3$ cm/s)	$D_{e,p}$ ($\times 10^6$ cm^2/s)	τ_p
2	0.79	200	8.35	2.016	1.69	3.32	1.45	3.71	1.7
3	0.79	200	5.44	1.008	1.97	3.46	1.38	3.16	2.0
4	0.79	200	8.59	1.006	4.32	4.25	2.10	3.09	2.1
5	0.79	200	22.4	1.014	16.4	5.94	1.76	2.96	2.2
6	0.79	200	16.4	0.800	12.0	5.22	0.98	2.84	2.2
7	0.79	200	16.6	1.301	9.85	5.07	2.63	2.87	2.2
8	0.79	200	15.8	2.601	4.67	4.34	1.23	3.09	2.1
9	0.79	200	3.37	1.001	0.70	2.57	0.93	3.23	2.0
10	0.79	100	3.37	1.001	0.75	2.63	0.73	2.81	2.3
12	0.65	200	5.63	1.007	1.76	3.76	1.30	2.78	2.3
13	1.29	200	5.66	1.004	2.21	2.93	3.07	3.31	1.9
14	0.79	150	7.28	1.001	3.32	3.97	0.37	2.73	2.3
15	0.79	200	7.65	1.003	3.89	3.72	0.73	2.78	2.3
16	0.79	250	9.11	1.004	4.71	4.35	0.78	3.31	1.9

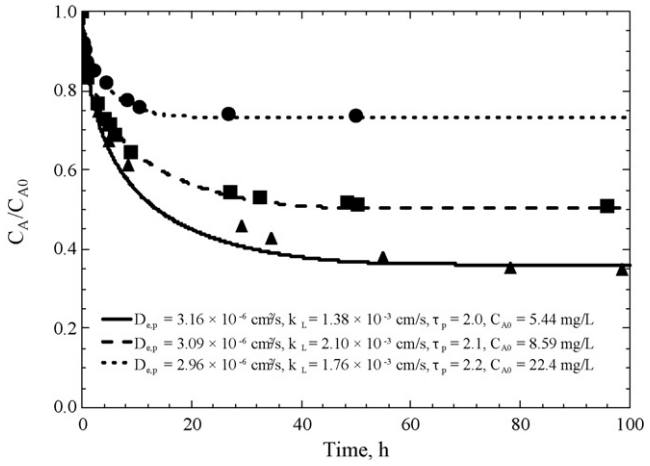

Fig. 2. Concentration decay curves for fluoride adsorption on bone char. The lines represent the diffusional model predictions. Run Nos. 3, 4 and 5.

The experimental values of $D_{e,p}$ are reported in Table 2 and vary between 2.73×10^{-6} and 3.71×10^{-6} cm^2/s.

The tortuosity factor of bone char can be estimated with the following equation [9,14]:

$$D_{e,p} = \frac{\varepsilon_p D_{F^-}}{\tau_p} \tag{28}$$

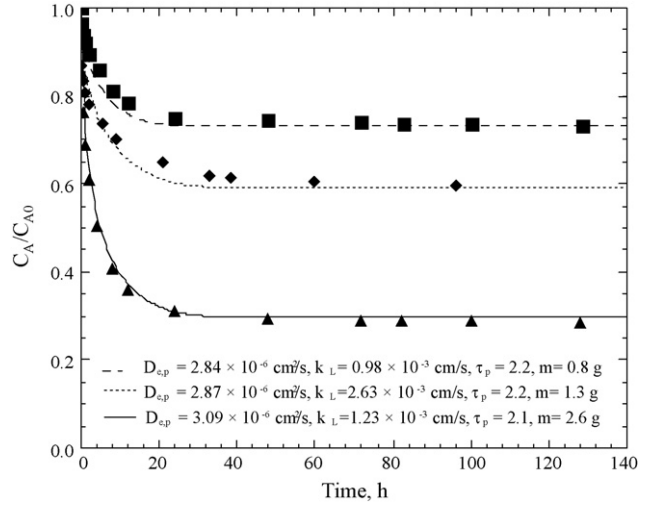

Fig. 3. Concentration decay curves for fluoride adsorption on bone char. The lines represent the diffusional model predictions. Run Nos. 6, 7 and 8.

The ionic diffusivity of fluoride is $D_{F^-} = 1.39 \times 10^{-5}$ cm^2/s (Section 5.3) and the value of the void fraction for the bone char is $\varepsilon_p = 0.46$ [29]. The values of the tortuosity factor, τ_p, estimated with Eq. (28) are shown in Table 2 and vary between 1.7 and 2.3. The rate of adsorption of heavy metals on bone char has been studied in several works [16,29,30] and it has been reported that the tortuosity factor of bone char varies between 2.7 and 3.6 [14,15].

Cheung et al. [14] studied the adsorption kinetics of Cd(II), Cu(II) and Zn(II) on bone char employing a film-pore diffusion model. The model was obtained by assuming that the rate of adsorption was controlled by the external mass transfer and pore volume diffusion. Furthermore, it was supposed that the adsorption of the metal took place on a shrinking core of the particle. Cheung et al. [30] reported that the experimental effective pore volume diffusivities of Cd(II), Cu(II) and Zn(II) were 0.528, 0.667 and 0.632×10^{-6} cm^2/s, respectively. These values are less than the effective diffusivity values of the fluoride ion. A possible explanation for this behavior is that the hydrated radius of the F^- (0.352 nm) [31] is less than those of the metal ions (the hydrated radii of Cd(II), Cu(II) and Zn(II) ions are 0.426, 0.419 and 0.430 nm, respectively). In other words, the fluoride ion diffuses faster than the metal ions because of its smaller size.

In general, it was observed that the experimental concentration decay data were reasonably well interpreted with the diffusional model and the variations of $D_{e,p}$ were not important. The arithmetic average of $D_{e,p}$ is 3.08×10^{-6} cm^2/s and the corresponding average tortuosity factor is $\tau_p = 2.1$.

The experimental concentration decay curves for run Nos. 2 and 10 are graphed in Fig. 4. For comparison purposes the concentration decay curves predicted with the diffusional model using the average value of $D_{e,p}$ ($D_{e,p} = 3.08 \times 10^{-6}$ cm^2/s) or average value of τ_p ($\tau_p = 2.1$) and with the best value of $D_{e,p}$ were also plotted in these figures. The experimental data of run Nos. 2 and 10 were chosen for this comparison because the best values of $D_{e,p}$ in these experiments correspond to the lowest and the highest values of τ_p (see Table 2). As seen in these figures, the fluoride concentration decay curves predicted with the average value of $D_{e,p}$ or τ_p are very similar to those predicted with the best value of $D_{e,p}$. Thus, the model prediction using the average tortuosity factor of $\tau_p = 2.1$ is also quite satisfactory.

5.6. Effect of the mass of fluoride adsorbed on $D_{e,p}$

The mass of fluoride adsorbed can affect the diffusion of fluoride inside the pores since the fluoride adsorbed on the pore surface might reduce the volume of the pore and block partially the pores. The effect of the mass of fluoride adsorbed at equilibrium, q_e, on D_{ep} was studied by carrying out experiments at the same conditions, but q_e was different in each experiment. This last condition was

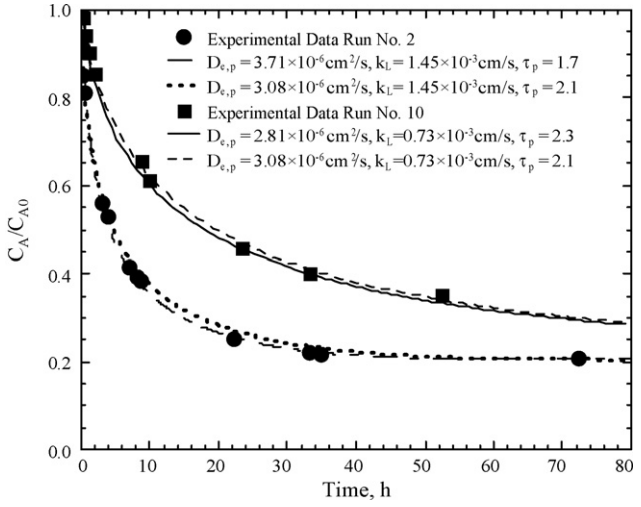

Fig. 4. Concentration decay curve for fluoride adsorption on bone char. The lines represent the diffusional model predictions. Run Nos. 2 and 10.

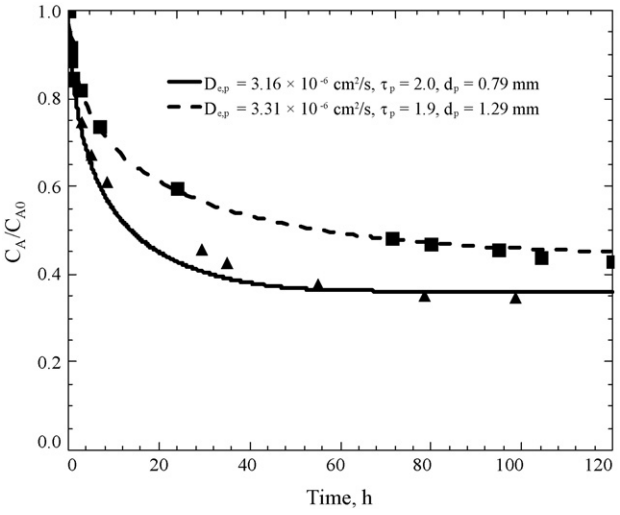

Fig. 6. Effect of the diameter particle on the fluoride concentration decay curves. The lines represent the diffusional model predictions. Run Nos. 3 and 13.

achieved by varying the initial concentration of fluoride or the mass of bone char. In each run, the final conditions at equilibrium, C_{A_e} and q_e, were calculated by solving the mass balance equation (9) and the adsorption isotherm equation (22).

The experimental concentration decay curves for run Nos. 3, 4 and 5 are graphed in Fig. 2 and these runs were carried out under the same conditions except that the initial fluoride concentration, C_{A_0}, was different in each run. Analyzing the experimental conditions of these runs in Table 2, it was noticed in that q_e increased when C_{A_0} was raised. This behavior is considered normal since the greater the amount of fluoride in the solution, the greater the amount of fluoride available for adsorption. The concentration decay curves for run Nos. 6, 7 and 8 are displayed in Fig. 3 and these runs were carried out at the same experimental conditions, but the mass of bone char, m, was varied in each run. The experimental conditions for these runs are given in Table 2. The values of q_e dropped as the mass of bone char increased because there was a greater mass of bone char per unit volume.

The effect of q_e on $D_{e,p}$ is shown in Fig. 5 and $D_{e,p}$ does not depend on q_e. This may be due to that q_e is very low and hence the fluoride adsorbed on the pore surface does not hinder fluoride diffusion in the pore volume.

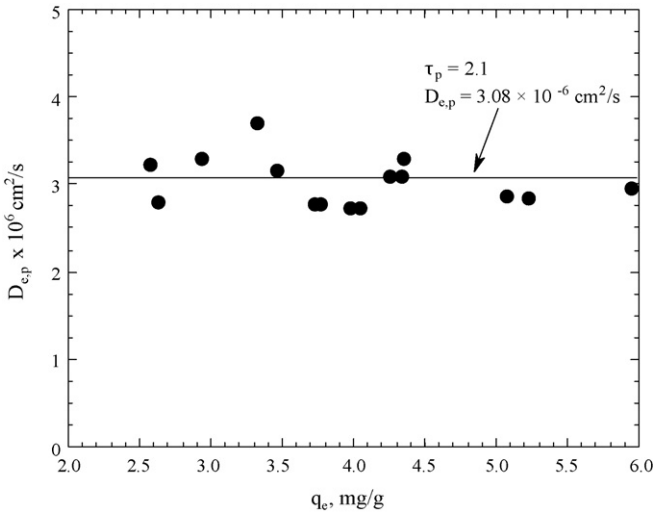

Fig. 5. Effect of the mass of fluoride adsorbed at equilibrium, q_e, on the effective diffusion coefficient, $D_{e,p}$.

5.7. Effect of the average particle diameter on the overall adsorption rate

The effect of the particle size on the overall adsorption rate was studied by obtaining the adsorption rate data using bone char particles with different particle diameters and keeping the rest of the experimental conditions constant. The experimental concentration decay curves for run Nos. 3 and 13 are shown in Fig. 6, and it can be noticed that adsorption equilibrium was attained faster by reducing the diameter of the bone char particles. This result implies that the overall adsorption rate increased while diminishing the diameter of the particle. This behavior was expected since the overall adsorption rate of fluoride was controlled by the intraparticle diffusion. If the particle diameter is smaller, then the distance traveled by the fluoride ion from the external surface to the active sites inside the pores will be shorter, resulting in a faster adsorption rate.

The experimental concentration decay curves for run Nos. 3 and 13 were predicted with the diffusional model and are plotted in Fig. 6. Again, the diffusional model satisfactorily interpreted the experimental data. The values of $D_{e,p}$ and τ_p varied very slightly with the particle diameter (see Table 2). Normally, the tortuosity of an adsorbent does not depend on the diameter of the particle but on its porous structure. This explains why τ_p does not depend on the particle diameter of bone char.

5.8. Importance of external mass transport in overall adsorption rate

In the rotating basket adsorber, the external mass transport depends on the impeller speed. The effect of the external mass transport in the overall adsorption rate was studied by performing experiments at the same experimental conditions but at different impeller speeds. The experimental concentration decay curves at the impeller speeds of 150, 200 and 250 rpm (run Nos. 14, 15 and 16) are graphed in Fig. 7, and it can be observed that in the first 3 h, the experimental concentration decay curve at 150 rpm is different from those at 200 and 250 rpm. Furthermore, the external transport coefficient, k_L, increased from 0.37 to 0.73 cm/s when the impeller speed was raised from 150 to 200 rpm (see Table 2, run Nos. 14 and 15). Thus, the external mass transport of fluoride was doubled by augmenting the impeller speed from 150 to 200 rpm. As seen in Fig. 7, the experimental concentration decay curve at the speed of 200 rpm is overlapping that at 250 rpm; this reveals that the external mass transport is no controlling the overall adsorp-

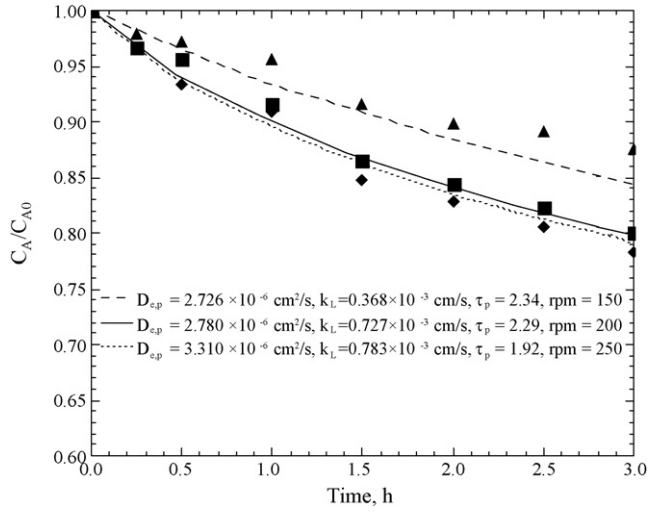

Fig. 7. Effect of the impeller speed on the concentration decay curves for fluoride adsorption on bone char. The lines represent the diffusional model predictions. Run Nos. 14, 15 and 16.

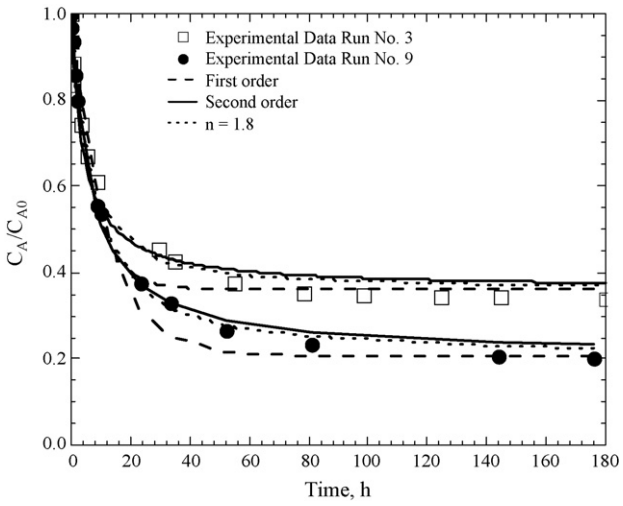

Fig. 8. Concentration decay curves for fluoride adsorption on bone char. The lines represent the kinetic model predictions. Run Nos. 3 and 9.

tion rate at speeds higher than 200 rpm. For this reason, the rest of experiments were performed at impeller speeds of 200 rpm.

5.9. Interpretation of the adsorption rate data with the kinetic models

The experimental data of the fluoride concentration decay curves were also interpreted with the kinetic models described earlier. The kinetic model equations for the first-, second- and *n*th-order were presented previously. The values of k_1 and k_2 were estimated by fitting the kinetic model to the experimental concentration decay data. The values of k_n and n of the *n*th-order kinetic model were obtained by matching the experimental concentration decay data with a numerical solution of the *n*th-order model computed by an integration method using the Scientist software. The best values of the rate constants (k_1, k_2 and k_n) and order (n) were estimated by a least-squares method using an optimization algorithm based upon the objective function represented by Eq. (27). The values of the kinetic parameters as well as the absolute average percentage deviation are given in Table 3.

The kinetic models are normally fitted to the experimental data by considering that the adjustable parameters are the rate constants (k_1, k_2 and k_n), the uptake at equilibrium (q_e) and the order (n) of the adsorption rate. In this work, q_e was not considered an adjustable parameter since it can be calculated as described in Section 5.6. If q_e is considered as an adjustable parameter then q_e cannot be predicted with the adsorption isotherm.

The experimental concentration decay curves for run Nos. 3 and 9 are presented in Fig. 8. The concentration decay data for the first-, second- and *n*th-order kinetic models are plotted as well. It is observed that the second- and *n*th-order kinetic models fit the experimental data well, whereas the first-order model does not. The absolute average percentage deviations vary between 0.5 and 7.1, 0.5 and 6.9 and 1.2 and 8.8%, for the *n*th-, second- and first-order models, respectively. The percentage deviations of the second-order model are very similar to those of the *n*th-order model and therefore, it was considered that both kinetic models fitted quite well the fluoride concentration decay data. The second-order kinetic model was chosen over the *n*th-order model because the values of the reaction order n varied considerably between 1.8 and 3.2 (see Table 3). Besides, the values of n varied without any trend concerning the operating conditions.

5.10. Dependence of the k_2 kinetic constant with regard to operating conditions

In Table 3 it is clearly noted that the rate constants (k_1, k_2 and k_n) varied considerably with the operating conditions (initial concentration of fluoride, mass of bone char, concentration of fluoride at equilibrium and mass of fluoride adsorbed at equilibrium) (see Table 2). The dependence of the rate constant k_2 with respect to

Table 3
Values of the rate constants for first-, second- and *n*th-order kinetic models.

Run No.	First-order		Second-order		*n*th-Order		
	k_1 ($\times 10^3$ min^{-1})	%*D*	k_2 ($\times 10^3$ g mg^{-1} min^{-1})	%*D*	k_n ($\times 10^3$ g^{n-1} mg^{1-n} min^{-1})	n	%*D*
2	3.5	8.6	2.2	6.9	2.0	2.0	7.1
3	2.3	6.5	1.2	6.2	1.3	1.8	5.0
4	3.1	4.6	1.3	3.2	1.1	2.2	3.6
5	6.8	3.2	2.3	1.6	1.0	2.7	1.5
6	3.0	1.9	1.0	0.8	0.9	2.1	0.8
7	7.3	5.7	2.4	3.4	0.7	3.1	3.0
8	7.1	7.3	2.9	4.4	2.8	2.1	4.6
9	1.4	7.5	1.0	5.7	1.1	1.8	4.5
10	0.9	8.3	0.6	4.1	0.7	1.8	3.3
12	4.2	8.5	1.6	4.1	1.3	2.3	4.6
13	1.2	8.8	0.6	4.6	0.5	2.5	4.7
14	1.3	1.2	0.4	0.7	0.2	2.5	0.7
15	2.6	2.8	0.9	1.5	0.3	3.2	1.2
16	3.2	1.6	1.0	0.5	0.9	2.1	0.5

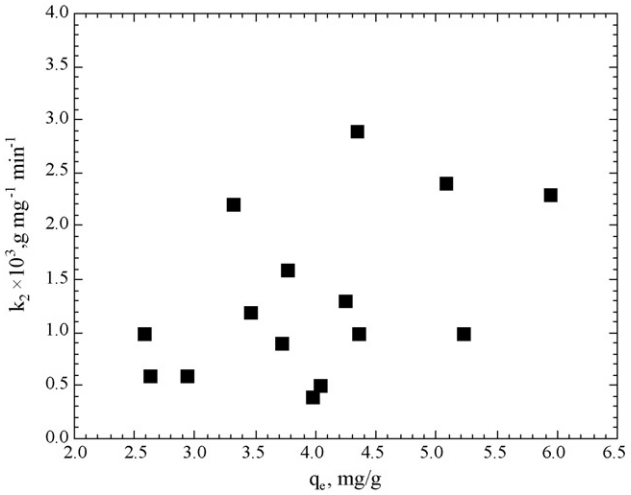

Fig. 9. Effect of the mass of fluoride adsorbed at equilibrium, q_e, on the rate constant k_2.

the mass of fluoride adsorbed at equilibrium is illustrated in Fig. 9 and similar behavior was also observed for the effect of the other operating conditions on k_2. It is considered that the second-order kinetic model interprets the fluoride concentration decay curves satisfactorily, but the k_2 constant varies without any trend regarding the operating conditions of the system. Therefore, k_2 cannot be predicted from the operating conditions and this behavior can drastically restrict the application of the kinetic model to predict the adsorption rate of fluoride on bone char.

5.11. Comparison of the diffusional model with the second-order kinetic model

The experimental concentration decay curves for fluoride adsorption on bone char are plotted in Fig. 10 for run Nos. 2 and 10, respectively. For comparison the concentration decay curves predicted with the second-order kinetic and diffusional models were also shown in these figures. In the case of the diffusional model, the concentration decay curves were predicted using the average values of $D_{e,p} = 3.08 \times 10^{-6}$ cm^2/s and $\tau_p = 2.1$. As indicated previously, these runs were selected because the best values of $D_{e,p}$ for these runs were the lowest and the highest values.

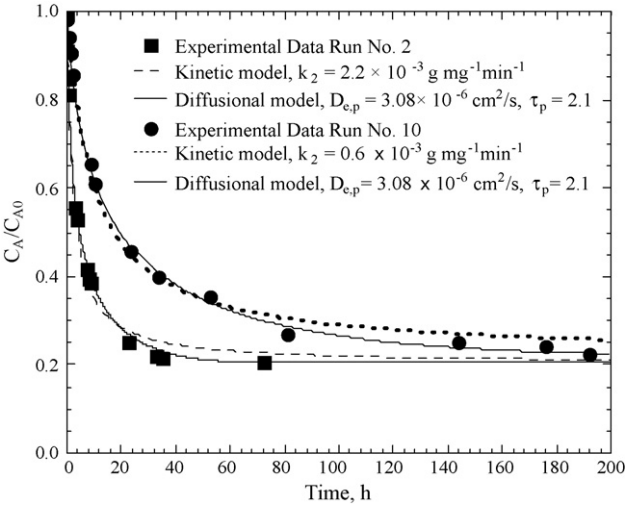

Fig. 10. Comparison of the concentration decay curves predicted with the diffusional model and the second-order kinetic model. Run Nos. 2 and 10.

Fig. 10 shows that both models interpret the experimental concentration decay curves quite well; however, the diffusional model fitted the experimental data slightly better. Besides, the constants of the kinetic model cannot be related to the experimental conditions and varied without any trend, and their variations have no physical meaning. Despite this fact, the kinetic models have been extensively used to interpret the adsorption rate because they are very simple and easy to use. On the other hand, the diffusional model is more complex to solve since it involves solving a partial and an ordinary differential equations. Moreover, it is considered that in these models, the external mass transport and specially the intraparticle diffusion play a very important role.

6. Conclusions

The diffusional model which assumes that intraparticle diffusion is the controlling step, adjusted satisfactorily the experimental data for the fluoride concentration decay curves. The external mass transport is quite fast and does not control the overall rate of adsorption. The kinetics of fluoride adsorption on bone char is predominantly controlled by the pore volume diffusion.

It was also found that the effective pore volume diffusivity does not depend on the mass of fluoride adsorbed at equilibrium. This result can be explained considering that the mass of fluoride adsorbed was low and the fluoride ions adsorbed on the pore surface do not block the pores.

The tortuosity factor of bone char was estimated from the experimental values of the effective pore volume diffusivity, the ionic diffusion coefficient of the fluoride in an aqueous solution and the void fraction of the bone char. The tortuosity factor varied between 1.7 and 2.3, and it is recommended to use a tortuosity factor of 2.1.

The second- and *n*th-order kinetic models fitted satisfactorily the experimental concentration decay curves of fluoride; nevertheless, the values of the kinetic constants and the order *n* varied considerably with the operating conditions. Moreover, the variation of the kinetic parameters did not exhibit any explainable trend.

References

[1] J. Fawell, K. Bailey, J. Chilton, E. Dahi, L. Fewtrell, Y. Magara, Fluoride in Drinking Water, IWA Publishing, London, UK, 2006.
[2] S. Ayoob, A.K. Gupta, T.B. Venugopal, A conceptual overview on sustainable technologies for defluoridation of drinking water, Crit. Rev. Environ. Sci. Technol. 38 (2008) 401–470.
[3] H. Mjengera, G. Mkongo, Appropriate defluoridation technology for use in fluorotic areas in Tanzania, Phys. Chem. Earth 28 (2003) 1097–1104.
[4] D.L. Mwaniki, Fluoride sorption characteristics of different grades of bone charcoal, based on batch tests, J. Dent. Res. 71 (6) (1992) 1310–1315.
[5] P. Phantumvanit, R.Z. Legeros, Characteristics of bone char related to efficacy of fluoride removal from highly-fluoridated water, Fluoride 30 (4) (1997) 207–218.
[6] I. Abe, S. Iwasaki, T. Tokimoto, N. Kawasaki, T. Nakamura, S. Tanada, Adsorption of fluoride ions onto carbonaceous materials, J. Colloid Interf. Sci. 275 (2004) 35–39.
[7] N.A. Medellin-Castillo, R. Leyva-Ramos, R. Ocampo-Perez, R.F. Garcia de la Cruz, A. Aragon-Piña, J.M. Martinez-Rosales, R.M. Guerrero-Coronado, L. Fuentes-Rubio, Adsorption of fluoride from water solution on bone char, Ind. Eng. Chem. Res. 46 (2007) 9205–9212.
[8] N.A. Medellin-Castillo, Equilibrio y cinetica de adsorcion de fluoruro sobre carbon de hueso, Ph.D. Thesis, Universidad Autonoma de San Luis Potosi, Mexico, 2009.
[9] R. Leyva-Ramos, J.R. Rangel-Mendez, L.A. Bernal-Jacome, M.S. Mendoza-Berber, Intraparticle diffusion of cadmium and zinc ions during adsorption from aqueous solution on activated carbon, J. Chem. Technol. Biotechnol. 80 (8) (2005) 924–933.
[10] M.S. Onyango, Y. Kojima, D. Kuchar, S.O. Osembo, H. Matsuda, Diffusion kinetic modeling of fluoride removal from aqueous solution by charge-reversed zeolite particles, J. Chem. Eng. Jpn. 38 (9) (2005) 701–710.
[11] R. Leyva-Ramos, C.J. Geankoplis, Model simulation and analysis of surface diffusion on liquids in porous solids, Chem. Eng. Sci. 40 (5) (1985) 799–807.
[12] C.W. Cheung, J.F. Porter, G. McKay, Elovich equation and modified second-order equation for sorption of cadmium ions onto bone char, J. Chem. Technol. Biotechnol. 75 (2000) 963–970.

[13] C.W. Cheung, J.F. Porter, G. McKay, Sorption kinetic analysis for the removal of cadmium ions from effluents using bone char, Water Res. 35 (3) (2001) 605–612.
[14] C.W. Cheung, C.K. Chan, J.F. Porter, G. McKay, Combined diffusion model for the sorption of cadmium, copper, and zinc ions onto bone char, Environ. Sci. Technol. 35 (2001) 1511–1522.
[15] C.W. Cheung, J.F. Porter, G. McKay, Removal of Cu (II) and Zn (II) ions by sorption onto bone char using batch agitation, Langmuir 18 (2002) 650–656.
[16] K.K.H. Choy, D.C.K. Ko, C.W. Cheung, J.F. Porter, G. McKay, Film and intraparticle mass transfer during the adsorption of metal ions onto bone char, J. Colloid Interf. Sci. 271 (2004) 284–295.
[17] D.C.L. Ko, C.M. Cheung, J.F. Porter, A branched pore kinetic model applied to the sorption of metal ions on bone char, J. Chem. Technol. Biotechnol. 80 (2005) 861–871.
[18] A. Sivasamy, K.P. Singh, D. Mohan, M. Maruthamuthu, Studies on defluoridation of water by coal-based sorbents, J. Chem. Technol. Biotechnol. 76 (7) (2001) 717–722.
[19] Y. Ku, H.-W. Chiou, The adsorption of fluoride ion from aqueous solution by activated alumina, Water Air Soil Pollut. 133 (2002) 349–360.
[20] S. Ayoob, A.K. Gupta, P.B. Bhakat, V.T. Bhat, Investigations on the kinetics and mechanisms of sorptive removal of fluoride from water using alumina cement granules, Chem. Eng. J. 140 (2008) 6–14.
[21] S. Ghorai, K.K. Pant, Equilibrium, kinetics and breakthrough studies for adsorption of fluoride on activated alumina, Sep. Purif. Technol. 42 (2005) 265–271.
[22] Y. Liu, Y.-J. Liu, Biosorption isotherms, kinetics and thermodynamics, Sep. Purif. Technol. 61 (2008) 229–242.
[23] J. Warna, M. Ronnholm, T. Salmi, K. Keikko, Application of CFD on a catalytic rotating basket reactor, Comp. Aided Chem. Eng. 10 (2002) 1009–1014.
[24] R. Leyva-Ramos, J.H. Soto-Zuñiga, J. Mendoza-Barron, R.M. Guerrero-Coronado, Adsorption of phenol from aqueous solution onto activated carbon. Effect of solvent, temperature and particle size, Adsorp. Sci. Technol. 17 (7) (1999) 533–543.
[25] P. Vanysek, Ionic conductivity and diffusion at infinite dilution, in: D.R. Lide (Ed.), CRC Handbook of Chemistry and Physics. A Ready-Reference Book of Chemical and Physical Data, 87th ed., CRC Press, Boca Raton, FL, USA, 2006.
[26] E.L. Cussler, Diffusional Maons on the kinetics and mechanisms of sorptive removal of fluoride from water using alumina cement granules, Chem. Eng. J. 140 (2008) 6–14.
[21] S. Ghorai, K.K. Pant, Equilibrium, kinetics and breakthrough studies for adsorption of fluoride on activated alumina, Sep. Purif. Technol. 42 (2005) 265–271.
[22] Y. Liu, Y.-J. Liu, Biosorption isotherms, kinetics and thermodynamics, Sep. Purif. Technol. 61 (2008) 229–242.
[23] J. Warna, M. Ronnholm, T. Salmi, K. Keikko, Application of CFD on a catalytic rotating basket reactor, Comp. Aided Chem. Eng. 10 (2002) 1009–1014.
[24] R. Leyva-Ramos, J.H. Soto-Zuñiga, J. Mendoza-Barron, R.M. Guerrero-Coronado, Adsorption of phenol from aqueous solution onto activated carbon. Effect of solvent, temperature and particle size, Adsorp. Sci. Technol. 17 (7) (1999) 533–543.
[25] P. Vanysek, Ionic conductivity and diffusion at infinite dilution, in: D.R. Lide (Ed.), CRC Handbook of Chemistry and Physics. A Ready-Reference Book of Chemical and Physical Data, 87th ed., CRC Press, Boca Raton, FL, USA, 2006.
[26] E.L. Cussler, Diffusional Mass Transfer in Fluid Systems, Cambridge University Press, USA, 1997.
[27] T. Furusawa, J.M. Smith, Fluid-particle and intraparticle mass transport rates in slurries, Ind. Eng. Chem. Fundam. 12 (1973) 197–203.
[28] M. Suzuki, K. Kawazoe, Particle to liquid mass transfer in a stirred tank with basket impeller, J. Chem. Eng. Jpn. 8 (1975) 79–81.
[29] N.A. Medellin-Castillo, Remocion de fluoruros en solucion acuosa sobre varios materiales adsorbentes, M.S. Thesis, Universidad Autonoma de San Luis Potosi, Mexico, 2006.
[30] C.W. Cheung, D.C.K. Ko, J.F. Porter, G. McKay, Binary metal sorption on bone char mass transport model using IAST, Langmuir 19 (2003) 4144–4153.
[31] E.R. Nightingale Jr., Phenomenological theory of ion solvation effective radii of hydrated ions, J. Phys. Chem. 63 (1959) 1381–1387.